ChemComm

Crystal Melting and Glass Formation in Copper Thiocyanate based Coordination Polymers

Journal:	*ChemComm*
Manuscript ID	CC-COM-03-2019-002172.R1
Article Type:	Communication

COMMUNICATION

Crystal Melting and Glass Formation in Copper Thiocyanate based Coordination Polymers

Received 00th January 20xx,
Accepted 00th January 20xx

DOI: 10.1039/x0xx00000x

Sanjog S. Nagarkar,[a] Haruna Kurasho,[b] Nghia Tuan Duong,[c] Yusuke Nishiyama,*[c,d] Susumu Kitagawa,[e] and Satoshi Horike*[a,b,e,f]

Crystal melting and glass formation of coordination polymers (CPs) and metal-organic frameworks (MOFs) are rare thermal events. To expand the library of melting CP/MOFs, we utilized anti-crystal engineering in ionic liquids to construct CPs. Combination of Cu^+ and 4,4'-bipyridin-1-ium derivatives afforded four melting CPs showing stable liquid and glassy states.

Glass is amorphous solid with lack of periodicity in atomic structure, commonly obtained by cooling the liquid, fast enough avoiding crystallization.[1] Optical transparency, structural isotropy and dynamics, mechanical flexibility are important properties of glasses.[2] Exploration of melting behaviour of coordination polymers (CPs), metal-organic frameworks (MOFs) has attracted much attention in recent as fundamentally new class of glass forming material.[3] CP/MOFs are constructed from coordination bonds, and most of reported CP/MOFs in liquid/glassy states preserve the identical coordination geometry in crystalline state.[4] Because of the unique liquid/glass topology in structures, they have showed functions of ion conductivity and porosity for instances.[4, 5, 6]

Nevertheless, of their potentials, there is little knowledge and thus library about how to synthesize a melting and glass forming CP/MOF crystals. For example, substitution of pendant $–CH_3$ group on ligand to –Cl in isostructural CPs leads to disappearance of melting behaviour, or both isostructural Zn^{2+} and Co^{2+} based zeolitic imidazolate frameworks (ZIFs) shows melting but Co^{2+} based metal-phosphate-azolates CP decompose without melting.[4, 6] Another report suggests use of bulky ligands in ZIFs to lower the melting temperature (T_m).[7] The initial insight in CP melting was provided by demonstrating applicability of Lindeman's rule.[4, 8] But some anomalous observations of glassy state of CP/MOFs[9] have suggested us the significance to explore another types of melting and glass forming CP/MOFs.

T_m is determined by intermolecular forces, molecular symmetry and conformational freedom present in the crystal.[10] There has been effort to control T_m in ionic liquids (ILs) which are composed of cations and anions, designed to reduce intermolecular interactions and avoid solid phase crystallization.[11] Coulomb interactions should be strong enough to keep ions in liquid state without decomposition. In general, ions with reduced symmetry and delocalized charge are used to synthesize ILs.[12] Reduced symmetry hinders ordered arrangements, whereas delocalized charge weakens the stronger electrostatic interactions. As referred from ILs, an anti-crystal engineering strategy is useful to control T_m in CP crystals.[13] Since most of CPs showing melting behaviour upon heating are constructed from Zn^{2+}, we here tried to synthesize with Cu^+ to expand the available metal ions. As a ligand, we employed thiocynate (SCN^-) having delocalized charge with variety of coordination modes and is also known to form ILs.[14] As co-ligands, a series of 4,4'-bipyridin-1-ium derivatives having lower symmetry were used.

Ligands 1-ethyl-[4,4'-bipyridin]-1-ium thiocyante (C_2bpySCN) and 1-butyl-[4,4'-bipyridin]-1-ium thiocyante (C_4bpySCN) were synthesized by alkylation of 4,4'-bipyridine in acetonitrile via modified literature procedure.[15] Aromatic substituted ligands 1-phenyl-[4,4'-bipyridin]-1-ium thiocyanate (PhbpySCN) and [3,1':4',4''-terpyridin]-1'-ium thiocyanate (3-PybpySCN) were synthesized by reacting Zincke salt of 4,4'-bipyridine with aniline and 3-aminopyridine respectively, in ethanol.[16] Using solvothermal reaction condition, four new CPs $[Cu_2(SCN)_3(C_2bpy)]$ (**1**), $[Cu_2(SCN)_3(C_4bpy)]$ (**2**), $[Cu_8(SCN)_{12}(Phbpy)_4]$ (**3**) and $[Cu(SCN)_2(3\text{-}Pybpy)]$ (**4**) were synthesized and characterized by single crystal X-ray diffraction (Fig. 1). **1**, **2** and **3**, contain two tetrahedral Cu^+ bridged by SCN^- via S,N-bridging to form distorted rectangular dimeric $Cu_2(SCN)_2$ cluster (Fig. 1a-1c). The dimeric clusters are connected by

[a] AIST-Kyoto University Chemical Energy Materials Open Innovation Laboratory (ChEM-OIL), National Institute of Advanced Industrial Science and Technology (AIST), Yoshida-Honmachi, Sakyo-ku, Kyoto 606-8501, Japan
[b] Department of Synthetic Chemistry and Biological Chemistry, Graduate School of Engineering, Kyoto University, Katsura, Nishikyo-ku, Kyoto 615-8510, Japan
[c] NMR Science and Development Division, RIKEN SPring-8 Center and Nano-Crystallography Unit, RIKEN-JEOL Collaboration Center, Tsurumi, Yokohama, Kanagawa 230-0045, Japan
[d] JEOL RESONANCE Inc., 3-1-2 Musashino, Akishima, Tokyo 196-8558, Japan
[e] Institute for Integrated Cell-Material Sciences, Institute for Advanced Study, Kyoto University, Yoshida-Honmachi, Sakyo-ku, Kyoto 606-8501, Japan
[f] Department of Materials Science and Engineering, School of Molecular Science and Engineering, Vidyasirimedhi Institute of Science and Technology, Rayong 21210, Thailand

Electronic Supplementary Information (ESI) available: Experimental Details, Crystallographic data, XRPD, DSC, IR, NMR. Crystallographic data for the compounds in CIF format with CCDC reference numbers 1899561-1899564. See DOI: 10.1039/x0xx00000x

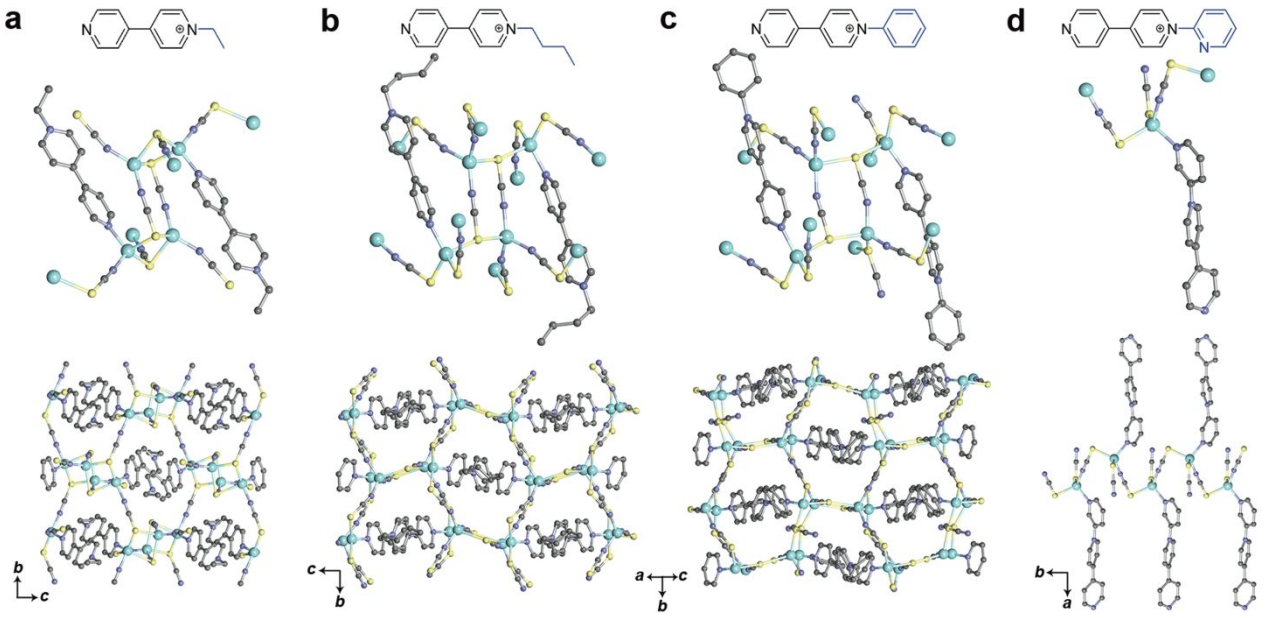

Fig. 1. Coordination environment and extended structure of (a) **1**, (b) **2**, (c) **3**, (d) **4**. The element Cu, N, S and C atoms are shown in sky blue, purple, yellow and grey colours respectively. H atoms were omit-ted for clarity.

bridging tetrahedral Cu^+ via S,S-bridging mode of sulphur atom present at the vertices of the dimeric cluster forming 2D anionic $[Cu_2(SCN)_3]_n^{n-}$ faveolated structure.[14] The overall negative charge is balanced by coordination of respective 4,4'-bipyridin-1-ium-based cationic ligands to bridging Cu^+ from opposite sides of the sheet. All three compounds maintained Cu^+, SCN^- and pyridinium ligand stoichiometry of 2:3:1. **4** has 1D chain structure with tetrahedral Cu^+ connected by SCN^- via S,N-bridging mode to form anionic $[Cu(SCN)_2]_n^{n-}$ helical chain (Fig. 1d). The pyridine functionality on meta position from 3-pybpy and additional SCN^- coordinate Cu^+ via S completing coordination environment. All four compounds were synthesized as a bulk crystalline powder in pure phase. X-ray powder diffraction (XRPD) patterns are in agreement with the respective XRPD patterns in simulation obtained from their single crystal structures (Fig. S1).

We carried out thermal analyses to study the phase transition. No significant weight loss was observed before decomposition ca. 205, 205, 235 and 250 °C (T_d) for **1**, **2**, **3** and **4** respectively in thermo-gravimetric analysis (TGA) (Fig. 2a). Differential scanning calorimetry (DSC) measurements showed endothermic peaks below T_d and following *in-situ* monitoring of sample morphology, the peaks were assigned to crystal melting (Fig. 2b, 2d). T_m for **1** and **4** are 187 and 203 °C. Highest T_m is for **3** (217 °C). Two endothermic peaks at 138 and 160 °C were observed for **2**, of which 138 °C is assigned to T_m followed by liquid to liquid transition at 160 °C.[17] The overall trend for T_m is **3** > **4** > **1** > **2**. The crystal melting in CPs is influenced by the substituent group on pyridinium ligands. The increase in alkyl chain length by two carbon atoms in **2** as compared to **1** resulted in similar structure with slight increase in the inter-layer spacing from 14 to 15 Å. In general, the increase in alkyl chain length increases the asymmetry in system with decrease in lattice energy. Thus less energy is required for melting **2** as compared to **1**. This relates to the thermal behaviour of ILs; where the lattice potential energies decrease with increasing alkyl chain length resulting in lowering of T_m.[18] Observation is

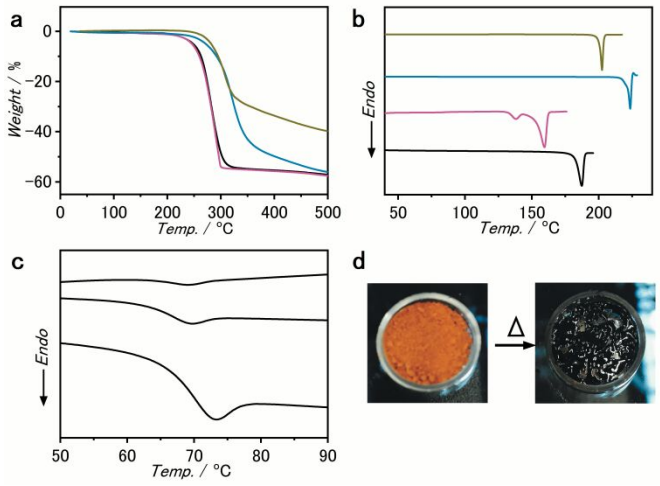

Fig. 2. (a) TGA and (b) First DSC heating up-scans of **1** (black), **2** (pink), **3** (blue), **4** (olive) under the N_2 atmosphere with heating rate of 10 °C min^{-1}. (c) Second DSC heating up-scans of **1**. Heating rates are 5 °C min^{-1} (upper), 10 °C min^{-1} (middle), and 20 °C min^{-1} (lower). (d) Picture of polycrystalline powder samples (**1**) and molten (**1**$_m$) sample formed on heating.

also supported by melting enthalpy (ΔH_m) and entropy (ΔS_m) recorded for CPs (Table S1). For **3**, the inter layer distance remain same as **2**, the π···π interaction between the pendent phenyl rings from adjacent 2D layers and between pyridinium rings of same layers provide additional stability to **3** resulting in highest T_m. However, the interactions are not too strong to suppress melting. For **4**, although the structure is 1D, both pyridinium and adjacent pyridine ring (N at para position) take

part in π···π interactions with rings from neighbouring chains and stabilizes the structure. These interactions are stronger than Van der Waal interactions present in **1** and **2**, resulting in higher T_m compared to **1** and **2**.[19] Higher structural dimensionality of **3** (2D) result in higher T_m than **4** (1D).[3]

TGA and DSC suggest that stable liquid state exists for all the compound between: 187-205 °C (**1**), 160-205 °C (**2**), 224-235 °C (**3**), and 203-250 °C (**4**) and become glassy on cooling to room temperature. During second heating cycle, the amorphous solids showed presence of glass transition (T_g) at 68 (**1**), 59 (**2**), 71 (**3**), and 72 (**4**) °C (Fig. S2). With increasing heating rates for **1**, the T_g shift to higher temperature with increase in area under the peak (Fig. 2c). This is due to the kinetic nature of T_g, where the fast heating rates prevent recovering the enthalpy or structural relaxation confirming the glassy nature.[20] T_g/T_m values for **1**-**4** are 0.74, 0.77, 0.69 and 0.73 respectively, which are in agreement with the empirical 2/3 rule followed by various glass forming systems.[21] Higher T_g/T_m implies resistance to crystallization and higher glass forming ability. Similar to poly(methyl methacrylate) glass, for example, the alkyl chains in **1** and **2** are expected to have higher degree of rotational freedom and the plasticizing effect resulting in better glass forming ability.[22] While for **3** and **4**, with dangling phenyl and pyridine rings, favourable π···π interactions are expected to promote the ordered structure.[9]

Variable temperature XRPD of **1** showed that the Bragg diffraction peaks become less intense below T_m and completely vanish upon further heating (Fig. S3). The profile remained featureless even when liquid state of **1** (**1**$_m$) was cooled to room temperature (**1**$_g$). Re-crystallization (**1**$_r$) of **1**$_g$ is feasible by a mechanical grinding by mortar. XRPD of **1**$_r$ showed overlapping crystalline pattern as that of **1** suggesting recovery of metal-ligand connectivity in **1**$_r$ identical to **1** (Fig. S4). For reversible structural transformation to occur, **1**$_g$ should maintain the reminiscent coordination geometry similar to **1**. To study the coordination environment of Cu^+ in **1**$_g$, we conducted Cu-*K*-edge X-ray absorption spectroscopy (XAS). X-ray absorption near-edge structure (XANES) spectra of **1** and **1**$_g$ displayed pre-edge feature at 8981 eV, assigned to the 1*s*→4*p* electronic transition of Cu^+ (Fig. 3a).[23] Presence of 1*s*⟶4*p* transition as a shoulder of the edge at 8987 eV in Cu^+ is a character of four coordinated Cu^+ along with Cu- S bond.[24] Higher absorption amplitude for pre-edge peak for **1**$_g$ than **1** suggest presence of few Cu^+ with decreased coordination number in **1**$_g$.[25] The decrease of white line intensity for **1**$_g$ relative to **1** also indicate lower symmetry

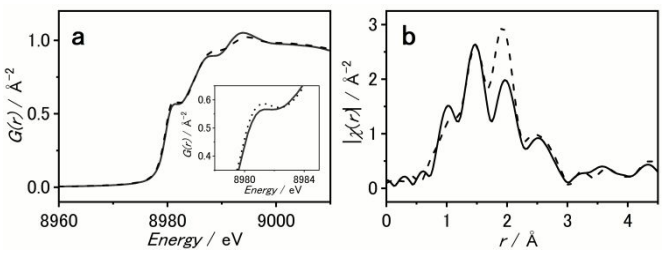

Fig. 3. (a) XANES spectra of **1** (solid line) and **1g** (dash line) observed at the K-edge of the Cu at 25 °C (Inset: Enlarged XANES spectra). (b) Corresponding EXAFS spectra extracted from XANES profile.

around Cu^+ in **1**$_g$. Both **1**, **1**$_g$ has monovalent Cu due to the absence of peak at 8978 eV, the mark of Cu^{2+}.[26] EXAFS (Extended X-ray Absorption Fine Structure) profile shows first coordination sphere of **1**$_g$ remains identical to **1**, and second and higher neighbouring atoms are closer and distorted (Fig. 3b).[27]

The C-N stretching frequency of SCN^- is sensitive to the nature of binding. The FT-IR of **1** and **1**$_r$ showed presence peaks corresponding to both S bonded and N bonded SCN^- moieties (2090, 2105 and 2110 cm^{-1}) in addition to bridging SCN^- (2125 cm^{-1}), consistent with crystal structure (Fig. S5).[28] Although the peak ascribed to both S bonded and N bonded SCN^- remains unaffected in FT-IR of **1**$_g$, the SCN^- bridging peak disappears with appearance of new peak corresponding to ionic SCN^- (2050 cm^{-1}).[29] This in agreement with the reduced coordination number of Cu^+ in **1**$_g$ revealed by XAS and partial retention of metal ligand connectivity.

Solid-state NMR spectra of **1** and **1**$_g$ showed quite similar ^1H and ^{13}C chemical shifts correlations in 2D $^1H/^{13}C$ and $^1H/^1H$ confirming the absence of chemical reaction during vitrification (Fig. 4a-4b, S6). The additional broadening in **1**$_g$ indicates the conformational distribution. Shorter ^1H T_1 relaxation time was observed in **1**$_g$ than in **1**, reflecting the higher molecular mobility (Table S2). The ^1H T_1 value of 3-6 s or absence of paramagnetic relaxation also supports that all Cu is monovalent. ^1H-^{63}Cu resonance echo saturation pulse double resonance (RESPDOR) experiments were carried out to determine the ^1H-^{63}Cu heteronuclear dipolar interactions, which is inversely proportional to cube of internuclear distances (Fig. 4c). Faster RESPDOR build up is observed if ^1H is located closer to ^{63}Cu. Aromatic proton shows much faster build up than CH_3 proton. In fact, while six of eight aromatic protons have Cu neighbour in a range between 3.0 to 3.6 Å, the distances between CH_3 proton and Cu is longer than 4.1 Å based on crystal structure of **1**. Similar RESPDOR build up curve is observed for CH_3 protons both in **1** and in **1**$_g$. This clearly shows the CH_3 groups maintain the similar structure after vitrification. On the other hand, build up curve of aromatic protons in **1**$_g$ are significantly slower than **1**. Weaker ^1H-^{63}Cu dipolar interaction in **1**$_g$ is associated with enhanced molecular motion and/or spatially loosen packing of aromatic rings. In order to probe the local ^1H-^1H network, ^1H T_2 relaxation time, which is dominated by the intense ^1H-^1H dipolar interactions in rigid solids, was measured (Table S3). While the T_2 relaxation time of CH_3 and CH_2 protons are close to each other in **1** and **1**$_g$, longer ^1H T_2 relaxation time is observed for aromatic protons in **1**$_g$ than in **1**. This indicates the vitrification does not change the ^1H-^1H strength at CH_2 and CH_3 positions, but weaken it at aromatic ring, agreeing with the ^1H-^{63}Cu RESPDOR experiments. This indicates the conformational distribution in **1**$_g$ is mainly ascribed to aromatic ring due to lack of π···π interactions. Phase transition is utilized to process the **1**$_g$ in to grain boundary-free transparent film (Fig. 4d).

As a conclusion, we synthesized four melting Cu^+-based CP crystals having either 2-D or 1-D extended structures from the ligands having delocalized charge and lower symmetry. The design is inspired by anti-crystal engineering in ionic liquids, and all of them possess stable liquid state regime which has been rare in CP/MOFs. We fabricated glassy state of them upon

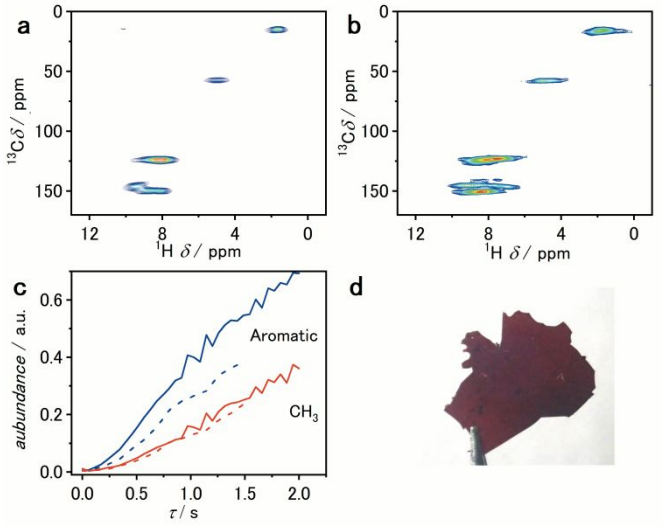

Fig. 4 2D $^{1}H/^{13}C$ correlation solid-state NMR spectra of (a) **1** and (b) $\mathbf{1}_g$. (c) ^{1}H-^{63}Cu RESPDOR build up curve, showing the strength of ^{1}H-^{63}Cu heteronuclear dipolar interactions for aromatic and CH_3 protons in **1** (solid line) and $\mathbf{1}_g$ (dashed line). (d) Monolith of $\mathbf{1}_g$ prepared by melt-quench.

gentle cooling. The CP glass maintains the coordination environment characterized by X-ray adsorption, and partial metal ligand connectivity similar to the crystal structure. The balance of iconicity, symmetry of metal ion/ligand, and tailored intermolecular interactions in CP are the key to observed stable liquid state. The present results contribute to share the information how to synthesize the melting CP/MOF crystals and expand the library of available metals centres.

The work was supported by the Japan Society of the Promotion of Science (JSPS) for a Grant-in-Aid for Scientific Research (B) (JP18H02032) from the Ministry of Education, Culture, Sports, Science and Technology, Japan, and Strategic International Collaborative Research Program (SICORP) and Adaptable and Seamless Technology Transfer Program through Target-driven R&D (A-STEP) from the Japan Science and Technology, Japan. We acknowledge Aichi Synchrotron Radiation Center BL5S1 beamline for XAS, and SPring-8 BL02B2 beamline for XRPD.

Conflicts of interest

There are no conflicts to declare.

References

1. C. A. Angell, *Science*, 1995, **267**, 1924; P. G. Debenedetti and F. H. Stillinger, *Nature*, 2001, **410**, 259; K. J. Rao, in *Structural Chemistry of Glasses*, ed. K. J. Rao, Elsevier Science Ltd, Oxford, 2002; S. Sen, *Adv. Phys.*, 2007, **56**, 1.
2. A. J. Ikushima, T. Fujiwara and K. Saito, *J. Appl. Phys.*, 2000, **88**, 1201; P. Boolchand and W. J. Bresser, *Nature*, 2001, **410**, 1070.
3. T. D. Bennett and S. Horike, *Nat. Rev. Mater.*, 2018, **3**, 431.
4. D. Umeyama, S. Horike, M. Inukai, T. Itakura and S. Kitagawa, *J. Am. Chem. Soc.*, 2015, **137**, 864.
5. R. Gaillac, P. Pullumbi, K. A. Beyer, K. W. Chapman, D. A. Keen, T. D. Bennett and F. X. Coudert, *Nat. Mater.*, 2017, **16**, 1149; S. S. Nagarkar, S. Horike, T. Itakura, B. Le Ouay, A. Demessence, M. Tsujimoto and S. Kitagawa, *Angew. Chem., Int. Ed.*, 2017, **56**, 4976.
6. L. Frentzel-Beyme, M. Kloß, R. Pallach, S. Salamon, H. Moldenhauer, J. Landers, H. Wende, J. Debus and S. Henke, *J. Mater. Chem. A*, 2019, **7**, 985.
7. T. D. Bennett, Y. Yue, P. Li, A. Qiao, H. Tao, N. G. Greaves, T. Richards, G. I. Lampronti, S. A. Redfern, F. Blanc, O. K. Farha, J. T. Hupp, A. K. Cheetham and D. A. Keen, *J. Am. Chem. Soc.*, 2016, **138**, 3484.
8. T. D. Bennett, J. C. Tan, Y. Yue, E. Baxter, C. Ducati, N. J. Terrill, H. H. Yeung, Z. Zhou, W. Chen, S. Henke, A. K. Cheetham and G. N. Greaves, *Nat. Commun.*, 2015, **6**, 8079.
9. A. Qiao, T. D. Bennett, H. Tao, A. Krajnc, G. Mali, C. M. Doherty, A. W. Thornton, J. C. Mauro, G. N. Greaves and Y. Yue, *Sci. Adv.*, 2018, **4**.
10. A. R. Katritzky, R. Jain, A. Lomaka, R. Petrukhin, U. Maran and M. Karelson, *Cryst. Growth Des.*, 2001, **1**, 261.
11. E. I. Izgorodina, Z. L. Seeger, D. L. A. Scarborough and S. Y. S. Tan, *Chem. Rev.*, 2017, **117**, 6696.
12. J. Dupont, *Acc. Chem. Res.*, 2011, **44**, 1223.
13. P. M. Dean, J. Turanjanin, M. Yoshizawa-Fujita, D. R. MacFarlane and J. L. Scott, *Cryst. Growth Des.*, 2009, **9**, 1137.
14. A. Di Santo, H. Perez, G. A. Echeverria, O. E. Piro, R. A. Iglesias, R. E. Carbonio, A. Ben Altabef and D. M. Gil, *RSC Adv.*, 2018, **8**, 23891.
15. M. Bonchio, M. Carraro, G. Casella, V. Causin, F. Rastrelli and G. Saielli, *Phys. Chem. Chem. Phys.*, 2012, **14**, 2710; A. Abebe, S. Admassie, I. J. Villar-Garcia and Y. Chebude, *Inorg. Chem. Commun.*, 2013, **29**, 210.
16. M. Christl, *Angew. Chem., Int. Ed.*, 2007, **46**, 9152; F. Lin, T.-Y. Zhou, T.-G. Zhan and X. Zhao, *Tetrahedron*, 2014, **70**, 2251.
17. Y. Katayama, T. Mizutani, W. Utsumi, O. Shimomura, M. Yamakata and K.-i. Funakoshi, *Nature*, 2000, **403**, 170.
18. H. Tokuda, K. Hayamizu, K. Ishii, M. A. B. H. Susan and M. Watanabe, *J. Phys. Chem. B*, 2005, **109**, 6103.
19. Q. M. Wang and D. W. Bruce, *Chem. Commun.*, 1996, 2505.
20. M. S. Dahiya, S. Khasa and A. Agarwal, *J. Mol. Struct.*, 2015, **1086**, 172.
21. K. Ito, C. T. Moynihan and C. A. Angell, *Nature*, 1999, **398**, 492.
22. K. J. B. A. Karim and N. A. Buang, *Polym. Rev.*, 2015, **55**, 678.
23. M. Giorgetti, L. Guadagnini, S. G. Fiddy, C. Santini and M. Pellei, *Polyhedron*, 2009, **28**, 3600.
24. I. J. Pickering, G. N. George, C. T. Dameron, B. Kurz, D. R. Winge and I. G. Dance, *J. Am. Chem. Soc.*, 1993, **115**, 9498.
25. L. S. Kau, D. J. Spira-Solomon, J. E. Penner-Hahn, K. O. Hodgson and E. I. Solomon, *J. Am. Chem. Soc.*, 1987, **109**, 6433.
26. C. Prestipino, L. Regli, J. G. Vitillo, F. Bonino, A. Damin, C. Lamberti, A. Zecchina, P. L. Solari, K. O. Kongshaug and S. Bordiga, *Chem. Mater.*, 2006, **18**, 1337.
27. M. Nomura and T. Yamaguchi, *J. Phys. Colloq.*, 1986, **47**, C8.
28. L. C. Nathan, *J. Chem. Educ.*, 1974, **51**, 285.
29. F. Jin, H.-P. Zhou, X.-C. Wang, Z.-J. Hu, J.-Y. Wu, Y.-P. Tian and M.-H. Jiang, *Polyhedron*, 2007, **26**, 1338.

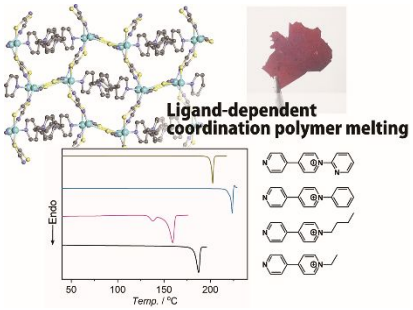

Melting point of Cu^{+} coordination polymer crystals is controlled by ligands, and the reversible crystal-to-glass states is observed.